SEMARAK ILMU PUBLISHING

Journal of Advanced Research in Fluid Mechanics and Thermal Sciences

Journal homepage:
https://semarakilmu.com.my/journals/index.php/fluid_mechanics_thermal_sciences/index
ISSN: 2811-3950

Dynamic Modeling and Simulation of the Forward Feed MED-TVC Desalination Plant

Somar Moaen Habib[1], Ahmed Hamed[1,*], Ahmed Yahia Youssef[1], Mahmoud Kassem[1], Abdalla Hanafi[1]

[1] Department of Mechanical Power Engineering, Cairo University, Egypt

ARTICLE INFO

Article history:
Received 1 October 2021
Received in revised form 6 January 2022
Accepted 11 January 2022
Available online 8 February 2022

Keywords:
Dynamic Modeling; Desalination; Forward Feed; MED-TVC; Simulation

ABSTRACT

The sudden disturbances in the operating parameters of desalination plants are common, especially when these plants are integrated with concentrated solar power (CSP). These disturbances damage the plants over time and may lead to a complete shutdown. This paper aims to investigate the performance of a forward feed multi-effect distillation plant with a thermal vapor compressor (FF-MED-TVC) which has a high potential for integration with concentrated solar power (CSP). However, the fluctuation and instability of solar energy require the development of dynamic model for the MED process to analyze the transient behavior. Few papers were published in the transient state, especially the forward feed (FF) configuration, as most of the papers focused on the parallel feed (PF) and parallel cross feed (PCF) configuration. Accordingly, a mathematical model has been developed using Engineering Equation Solver (EES) software and validated against data reported from two previous models in the literature, where a perfect agreement was obtained. Then the proposed model was employed to predict the system's response to the most important parameters that may change suddenly in the real operating environment, such as the variation in the motive steam pressure, feed seawater mass flow rate, and temperature. For the same percentage (10%) of these three disturbances, the results indicated that the needed time to return to 95 % of steady state is the longest in the case of increasing the seawater mass flow rate (about 350 seconds after the turbulence is removed), while it is the shortest in the case of increasing the pressure of motive steam (about 50 seconds after the turbulence is removed). In this paper, a comprehensive analysis of the transient performance was performed and a clearer view of the dynamic response was given which enables to optimize the control strategy and improve the stability.

1. Introduction

Recently, the water desalination market is in huge growth due to the rapid increase in the need for freshwater, whether for domestic use, industry, or agriculture, due to the increase in the population on the one hand and climatic changes on the other. For this purpose, many distillation technologies have been developed [1], such as distillation using electrical energy (ED), mechanical energy (Ro, MVC), and thermal energy which is the most common due to the complete purity of salt,

* *Corresponding author.*
E-mail address: ahamed@eng.cu.edu.eg

https://doi.org/10.37934/arfmts.92.1.190211

regardless of the salinity of seawater, in addition to the possibility of integration with Solar Rankin cycle power plants [2, 3], absorption chillers [4], heat pumps[5], the vapor-compression refrigeration systems [6], and solar energy technologies as a source of thermal energy [7, 8]. Among thermal desalination processes, the Multi-Effect Distillation (MED) technology is currently the most focused, due to the higher energetic performances achieved and the larger flexibility compared to the traditionally preferred Multi-Stage Flash (MSF) technology [9], also it requires relatively less pretreatment than RO [10].

The MED consists of a series of successive evaporators that differ from each other by the saturation pressure, in addition to the bottom condenser, and sometimes the MED is integrated with a series of successive preheaters to improve the gain output ratio (GOR) and reduce the total heat transfer area of the evaporators [11], also it can be integrated with thermal vapor compressor (TVC) where this procedure improves the GOR and improves energic performance by 30-40% compared to the same plant without the thermal compressor [10]. Several types of the MED plant differ from each other in the feed water and heating vapor flow directions, parallel feed (PF), parallel/cross feed (PCF), backward feed (BF), and forward feed (FF). In the forward feed (FF), which will be studied carefully in this paper, the feed water stream flows through the down condenser then passes through a series of preheaters, so that the feed water is heated up to reach the first effect. At the same time, the brine from each effect is used as the feed water in the next effect [1].

El-Dessouky *et al.,* [12] carried out a steady-state performance analysis that included PF and PCF-MED, and they concluded that the thermal performance of the PCF is higher than PF. Also, El-Dessouky and Ettouney [1] made a steady state performance analysis of each type of the four types in detail, but they made many assumptions for simplicity, neglected the effect of non-condensable gases, and did not study the presence of the preheaters or flash boxes. Shen *et al.,* [13] conducted a study of the PCF-MED-TVC plant in the steady state according to the same method as El-Dessouky *et al.,* [12] with some modifications and additions in order to show additional details, and they conducted a validation of their theoretical results with an actual data, they concluded that the increase of the motive pressure will increase each of the GOR, Ra, and specific exergy consumption, while each of the condenser inlet seawater mass flow rate, specific energy consumption, and specific heat transfer area will decrease. From other hand, the increase of the suction steam temperature will decrease each of the motive steam mass flow rate, specific energy and exergy consumption, and the condenser inlet seawater mass flow rate, while GOR and Ra will increase. Alamolhoda *et al.,* [14] investigated the performance of the PCF-MED-TVC plant by performing simulations to predict the influence of variation and disturbances of different input parameters on the system performance. By simultaneous solution of the mass and energy balance equations for each component of the station with an important studied disturbance, they gave a clearer view of the system's response, although the study neglected the presence of preheaters and non-condensable gases, they concluded that the increase of feed water flow rate will decrease each of the total product flow rate and GOR.

Hanafi *et al.,* [15] have carried out a thermo - economic model of a superstructure combined cogeneration power plant, where power plant has been integrated with a desalination plant FF-MED-TVC. The study aimed to assess the enhancement of the thermal performance, the environmental impact and the economics cost of the plant. Optimum design point for maximum production of power and water is obtained. Askari and Ameri [16] conducted a thermodynamic analysis of the PCF-MED-TVC plant to show the effect of the ejector's location, and the effect of changing the pressure of motive steam, in addition to some other parameters on the thermal performance and the total efficiency of the plant, they detected the optimal TVC location for different number of effects and pressures, and concluded that the decreasing of cooling seawater temperature will decrease the specific heat transfer area of the system, also the decreasing of the heating steam temperature will

increase the specific heat transfer area. Guo *et al.,* [11] have studied the effect of preheaters and their location and number on the GOR and the total heat transfer area in the plant. They studied the MTD desalination plant consisting of ten effects, and divided them into three groups so that the forward feed arrangement is adopted among groups and the parallel feed arrangement among evaporators in a specific group. Elsayed *et al.,* [17] performed thermo-economic analysis for the four configurations of MED-TVC which are all integrated with TVC, to determine the type with the best performance and to estimate the cost of water by applying the specific exergy cost flow method, they concluded that the PCF-MED has the highest GOR, and the lowest specific heat consumption, also has the lowest total power consumption, but it has a high specific cooling water flow rate.

Unfortunately, when it comes to the dynamic modelling of MED system literature, few papers can be found. Aly and Marwan [18] developed a good dynamic model for the MED plant, but they did not make any validation by experimental data. Mazini *et al.,* [19] improved the previous study [18] by reducing assumptions and increasing details to investigate the dynamic response of the PF-MED-TVC, and the model was validated by actual data from an operating plant, but they neglected the presence of non-condensable gases, and the proposed model does not contain preheaters or flash boxes. Cipollina *et al.,* [9] conducted a comprehensive analysis of the PF-MED-TVC plant which includes preheaters in the presence of non-condensable gases, but without flash boxes, then they performed a validation of the proposed dynamic model with actual data and obtained a close result. Guimard *et al.,* [20] extended their previous work [9] with some improvements such as introducing modified equations of non-condensable gases and brine connection between two successive effects in their model, modelling preheaters more accurately, and taking into account the accumulated heat in the tubes' wall, which made their results clearer and closer to the actual data.

Dong *et al.,* [21] made a dynamical modeling and simulation analysis of a nuclear desalination plant based on the PCF-MED-TVC plant which includes preheaters and flash box where all the components are proposed based upon the balance of mass, energy, momentum and salt, but they neglected the structural thermal inertia of the evaporators, preheaters and the down condenser compared to the high thermal inertia of the fluid. Georgiou and Bonanos [22] modeled transient behavior for FF-MED, but the studied plant was not integrated to TVC and there are no preheaters, and they did not mention the assumptions in building the code; additionally, the dynamic behavior was confined to the change in the amount of heat supplied to the circuit. Elsayed *et al.,* [10, 23] studied the four types of MED plant, and made a clear comparison between them, but only the type PCF-MED was integrated to TVC, also there are no preheaters.

It is noticed that the most published articles on dynamic modeling focus on PF/PCF MED and does not extend to the dynamic behavior of FF-MED-TVC plant. In this paper, the FF-MED-TVC plant which includes the steam jet ejector, falling film horizontal tube effect evaporators, end condenser, and preheaters are proposed based upon the balance of mass, energy, momentum and salt, to obtain a mathematical model which simulates the plant's energy performance and response to the most important disturbances that may occur in the real operation environment, especially when the station is integrated with a solar thermal system. A disturbance technique for seawater temperature, seawater mass flow rate, and motive steam pressure parameters have been done by using rectangular pulse forcing function to perform the dynamic input signal and to study the impact of these disturbances on the behavior of the other parameters, such as the distributions of the temperature, salt concentration, mass flow rates, and physical properties.

The model was validated against the steady-state performance of the data reported from two previous models in the literature. Later, the model was applied to predict the transient behavior of the plant.

2. System Description

Figure 1 shows a schematic diagram of FF-MED-TVC units. The total required rate of distillate is 1 kg/s. Motive steam, which is coming from steam generator at 2 bar, is supplied to the thermal vapor compression TVC. This steam is used to draw vapor from the last effect of the MED unit at a saturation temperature of 40°C and compress it to higher pressure and saturation temperature equals to 75 °C. The compressed steam enters the first effect tubes at TBT 70 °C, and the preheated feed water is supplied to the first effect at 65 °C. In the first effect tubes, the compressed steam is condensed, while the feed water is heated up to the saturation temperature of the first effect, then a small part of this feed water will evaporate while the rest (brine) will be introduced to the next effect as a feed water. The condensed vapor in the first effect tubes is returned back to steam generator, while the generated vapor in the first effect is partially condensed in the last preheater, where the feed water is heated up.

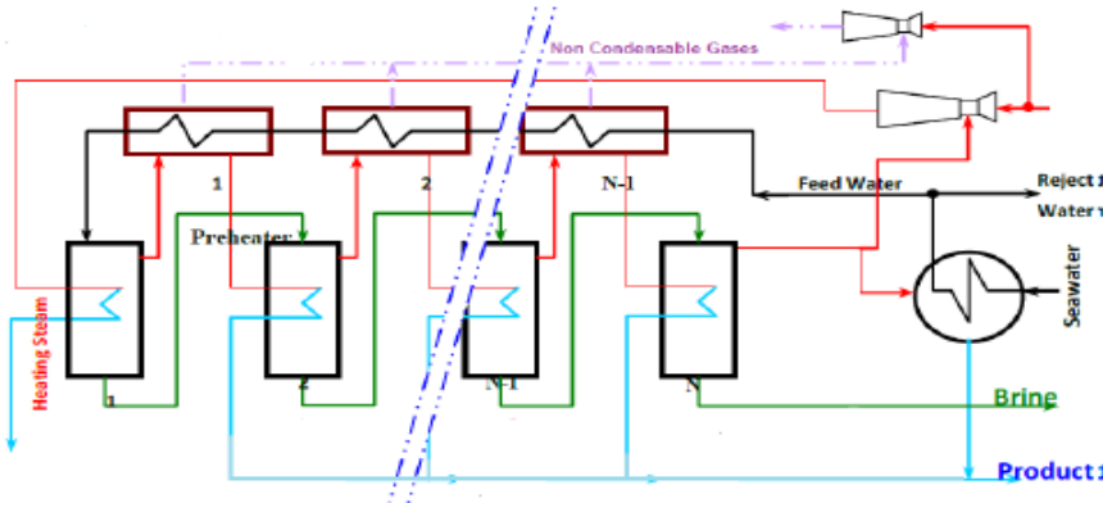

Fig. 1. Schematic diagram of FF-MED-TVC system

The vapor comes out of the preheater as wet vapor, then entering the second effect tubes, as a heating steam. The saturation temperature of the first effect is higher than that of the second effect by ΔT_{effect}. The heating steam coming from the first effect to the second effect is condensed inside its tubes, while a part of the feed water (brine) coming from the first effect is evaporated. This vapor is supplied to the next effect tubes as heating steam after it has partly condensed in the next preheater section, this cycle is repeated until reaches the last effect. In the last effect, a part of the generated vapor is entrained by TVC, while the remaining is supplied to the end condenser. The condensed vapor in the condenser is mixed with the final product, while the seawater is heated up. The seawater then divided into two parts, the first one is rejected to sea, while the second one represents the feed water which enters the preheaters up to reach the first effect. The parameters of MED-TVC are described in Table 1.

Table 1
Model parameters for FF-MED-TVC

Parameter	Value	Parameter	Value
The Productivity M_d, (kg/s)	1	Feed water temperature (°C)	65
Seawater salt concentration S_f, (ppm)	38500	Last effect temperature T_n, (°C)	40
Number of effects	6	Seawater temperature, (°C)	25
Top brine temperature TBT (°C)	70	The temperature difference between each successive phase ΔT_{eff}, (°C)	6
Number of preheaters	5	Motive steam pressure (bar)	2
Recovery ratio RR	0.4	Quality of motive steam	1

3. Dynamic Model

To improve the stability and operational efficiency of the plant and to develop optimal control strategies which prevent damage to the station as a result of an external disturbance occurs, it is necessary to create a dynamic model to get a better understanding of the plant's behavior under transient conditions. Therefore, the main hypothesis and the global structure of the model are:

i. The produced steam is salt-free.
ii. Heat losses to the surrounding environment are neglected.
iii. The vapor phase containing steam is assumed to be an ideal gas.
iv. There is no effect of non-condensable gases.
v. The physical properties of water and steam in each effect are calculated based on the saturation temperature in each effect.
vi. The steam ejector is modeled using steady-state equations.
vii. No vapor flashing takes place inside the effects.
viii. The driving force for heat transfer in each is effect equal to the difference between the condensation and evaporation temperatures only.
ix. No change in rejected water flow rate, so any disturbance in seawater flow rate will affect only the feed water at the first effect.
x. The condensate inside tubes are assumed to be complete and well-mixed.

Engineering Equation Solver "EES" code has been developed to solve both the steady-state and dynamic models equations, so that, the steady-state solution is used as the initial condition for the dynamic response calculations. The time step, which equals to (0.03) s, was chosen to have no effects on the stability of the results.

3.1 Mathematical Model of the Steam Jet Ejector

The ejector is a mechanical device used to compress the steam drawn from the last effect, so that it can be able to increase the plant energetic performance by 30–40% and reduce the amounts of needed motive steam, thus reducing the cooling water and pumping power [21]. The ejector consists of four main sections: convergent-divergent nozzle [24, 25], mixing chamber, throat, and diffuser. The motive steam enters the nozzle and accelerates to supersonic speed while its pressure drops, then the supersonic flow expands in the mixing chamber so that it can be able to draw a part of generated vapor in the last effect. Both the pressures and velocities of these two fluids are homogenized as the mixing completes, then the mixture enters the throat where a normal shock will

occur if the mixture is still supersonic, finally, the diffuser decelerates the mixture and increases its pressure to match it with the ejector exit pressure. The steam ejector is modeled just in steady-state because its response is much faster than each component of the desalination plant, where the mathematical model was developed by El-Dessouky and Ettouney [1].

In the case of steady-state, the pressure of the motive steam, entrained steam, and compressed steam are the inputs of the model, while the outputs are the entrainment ratio (Ra), the cross-section areas of the ejector, and the mass flow rates of entrained steam, motive steam, and the compressed steam that will enter the tubes of the first effect. In the case of a dynamic model, and after the geometric parameters of the ejector have been determined, the same equations can be used in a reverse procedure to predict the performance and response of the ejector when any disturbance occurs.

3.2 Mathematical Model of the Typical Effect Evaporator

Figure 2 shows a schematic diagram of the typical effect (i) in the FF-MED-TVC plant, where distillation and evaporation processes occur in each effect, each effect can be divided into three lumps, brine pool, vapor space, and tube bundle. The mass, energy and salt balance dynamic equations for each lump of the effect are determined [26, 19], where all effects have identical dynamic equations, except the first effect, last effect, and the condenser.

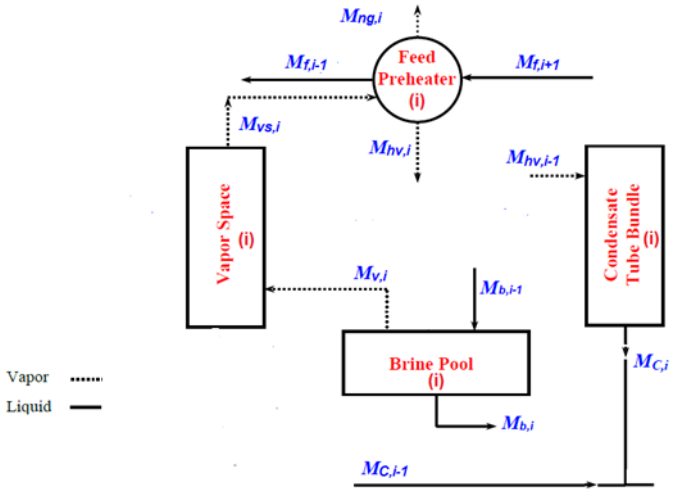

Fig. 2. Physical model of typical effect (i) in FF-MED plant

3.2.1 Brine pool

Mass balance for ith effect:

$$\frac{dm_{b,i}}{dt} = M_{b(i-1)} - M_{b,i} - M_{v,i} \quad (1)$$

where $m_{b,i}$, $M_{b,i}$ and $M_{v,i}$ are respectively the mass of accumulated brine flow, mass flow rate of brine, and the generated vapor in the effect.

Energy balance for ith effect:

$$m_{b,i}.\frac{dH_{b,i}}{dt} = M_{b(i-1)}.\left(H_{b(i-1)} - H_{b,i}\right) - M_{v,i}\,.\left(H_{v,i} - H_{b,i}\right) + Q_{ad(i)} \quad (2)$$

where $H_{b(i)}$, $H_{v,i}$, and $Q_{ad(i)}$ are respectively the enthalpy of brine, generated vapor, and the added heat to the brine pool, resulting from the condensation of the heating steam generated in the previous effect, which will be determined later.

And salt balance for ith effect:

$$m_{b,i} \cdot \frac{dS_{b,i}}{dt} = M_{b(i-1)} \cdot \left(S_{b(i-1)} - S_{b,i}\right) + S_{b,i}(M_{v,i}) \quad (3)$$

3.2.2 Vapor space

Mass balance for ith effect:

$$\frac{dm_{sv,i}}{dt} = M_{v,i} - M_{vs,i} \quad (4)$$

where $m_{sv,i}$ is the mass of accumulated vapor in the vapor space of effect (i).

Energy balance for ith effect:

$$\mathrm{m_{sv,i}} \cdot \frac{\mathrm{dH_{sv,i}}}{\mathrm{dt}} = M_{v,i}\left(H_{v,i} - H_{sv,i}\right) - M_{vs,i}(H_{vs,i} - H_{sv,i}) \quad (5)$$

3.2.3 Tube bundle

Mass balance for ith effect tube:

$$\frac{dm_{ct,i}}{dt} = M_{hv(i-1)} - M_{c,i} \quad (6)$$

where $M_{hv(i-1)}$, $M_{c,i}$ and $m_{ct,i}$ are respectively the mass flow rate of the heating steam coming from the previous preheater, condensate water, and the mass of accumulated condensate water in the tubes of effect (i).

Energy balance for ith effect tube:

$$m_{ct,i} \cdot \frac{dH_{ct,i}}{dt} = M_{hv(i-1)} \cdot \left(H_{hv(i-1)} - H_{ct,i}\right) - Q_{ad(i)} \quad (7)$$

3.3 Mathematical Model of Preheaters

Successive preheaters are used to raise the temperature of the feed water before it being dispersed in the first effect, which leads to an increase in the efficiency of the plant [11]. Each preheater can be divided into two lumps; preheater vapor space lump and preheater tube bundle lump, which are modeled and described in the following differential equations [26, 27].

3.3.1 Preheater tube bundle lump

Mass balance for preheater tube:

$$\frac{dm_{f,i}}{dt} = M_{f(i+1)} - M_{f(i-1)} \quad (8)$$

Energy balance equation of the preheater tube bundle is:

$$m_{f,i} \cdot \frac{dH_{f,i}}{dt} = M_{f(i+1)} \cdot \left(H_{f(i+1)} - H_{f,i}\right) + Q_{pre,i} \quad (9)$$

3.3.2 Preheater vapor space lump

Mass balance for preheater vapor space:

$$\frac{dm_{fh,i}}{dt} = M_{vs,i} - M_{hv,i} \quad (10)$$

And the energy balance equation of the preheater vapor space is:

$$m_{fh,i} \cdot \frac{dH_{fh,i}}{dt} = M_{vs,i} \cdot \left(H_{vs,i} - H_{fh,i}\right) - M_{hv,i} \cdot \left(H_{hv,i} - H_{fh,i}\right) - Q_{pre,i} \quad (11)$$

3.4 Mathematical Model of the End Condenser

Figure 3 shows a schematic diagram of the end condenser, where the generated steam by the last effect ($M_{v,n}$) is divided into two parts, the first one (M_B) is drawn by the ejector, and the second one (the rest) is condensed with seawater ($M_{sea,in}$) by end condenser, so that the seawater is heated, and a part of it is used as feed water ($M_{f,n}$) for the first effect, while the bulk (M_{cw}) is returned to the sea as cooling water.

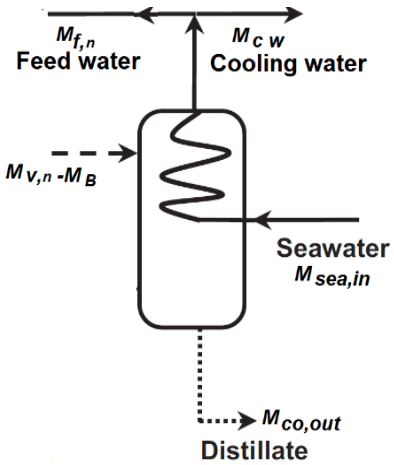

Fig. 3. Schematic diagram of the end condenser

The end condenser is divided into two lumps; condenser vapor space lump and condenser tube bundle lump which are modeled and described in the following differential equations [26, 27].

3.4.1 Condenser tube bundle lump

Mass balance for condenser tube

$$\frac{dm_c}{dt} = M_{sea,in} - M_{f,n} - M_{cw} \quad (12)$$

Energy balance equations of the condenser tube bundle are expressed by:

$$m_c \,.\frac{dH_c}{dt} \quad = \quad M_{sea,in}\,(\,H_{sea} - H_c) + \; Q_{rej,co} \tag{13}$$

where $Q_{rej,co}$ is the rejected heat to the seawater, which will be determined later.

3.4.2 Condenser vapor space lump

Mass balance of the vapor in the condenser can be determined by equation:

$$\frac{dm_{co,v}}{dt} \; = \; M_{v,n} - M_B - M_{co,out} \tag{14}$$

where $M_{co,out}$ is the mass flow rate of condensate water that exits from the end condenser.

Energy balance of the vapor space lump in the condenser:

$$\begin{aligned} m_{co,v}.\frac{dH_{co,v}}{dt} = \; & M_{v,n}\,.(H_{v,n} - H_{co,v}) - M_B.(H_{v,n} - H_{co,v}) - \\ & M_{co,out}.(H_{co,out} - H_{co,v}) - Q_{rej,co} \end{aligned} \tag{15}$$

3.5 Mathematical Model of the Heat Transfer Rates

Due to the low temperatures at which the plant operates, heat transfer by radiation will be neglected, and therefore heat is transferred from the hot fluid to the walls of tubes by convection, through the wall by conduction, and from the walls to the cold fluid by convection again, so that the differential equation of heat transfer between the two fluids inside any effect can be expressed by, [1, 26, 27]

$$\frac{d}{dt}Q_i = A_{in,i}.\left\{U_{in,i}.\left(\frac{d}{dt}T_{v,i-1} - \frac{d}{dt}T_{b,i}\right) + \frac{d}{dt}U_{in,i}.(T_{v,i-1} - T_{b,i})\right\} \tag{16}$$

The thermodynamic losses represented by the difference between the generated vapor temperature $T_{v,i}$ and brine pool temperature $T_{b,i}$ in each effect:

$$T_{b,i} = T_{v,i} + T_{BPE_i} \tag{17}$$

$$\begin{aligned} T_{BPE,i} = \; & \left(0.0825431 \quad + 0.0001883 \quad * T_{b,i} + 0.00000402 \quad * T_{b,i}^2\right) \quad S_{b,i} \\ & + \left(-0.0007625 \quad + 0.0000902 \quad * T_{b,i} - 0.00000052 \quad * T_{b,i}^2\right) \quad S_{b,i}^2 \\ & + \left(0.0001522 \quad - 0.000003 \quad * T_{b,i} + 0.00000003 \quad * T_{b,i}^2\right) \quad S_{b,i}^3 \end{aligned} \tag{18}$$

By differentiating the previous Eq. (17) with respect to the time (t):

$$\frac{d}{dt}T_{v,i} = \frac{d}{dt}T_{b,i} - \frac{d}{dt}T_{BPE,i} \tag{19}$$

By differentiating the previous

$$\begin{aligned}\frac{d}{dt}\left(T_{BPE,i}\right) &= \left(0.081 + 2.785 * 10^{-4} T_{b,i} + 3.5 * 10^{-6} * T_{b,i}^{2}\right)\frac{d}{dt}\left(S_{b,i}\right) \\ &+ \left\{\left(1.883 * 10^{-4} + 8.04 * 10^{-6} * T_{b,i}\right) + S_{b,i}\left(9.02 * 10^{-5} - 1.04 * 10^{-6} * T_{b,i}\right)\right. \\ &\left. + S_{b,i}^{2} * \left(-3.0 * 10^{-6} + 6.0 * 10^{-8} * T_{b,i}\right)\right\} S_{b,i}\frac{d}{dt}\left(T_{b,i}\right) \\ &+ \left(4.566 * 10^{-4} - 9.0 * 10^{-6} * T_{b,i} + 9.0 * 10^{-8} * T_{b,i}^{2}\right)\frac{d}{dt^{2}}\left(S_{b,i}^{2}\right)\end{aligned} \tag{20}$$

On the other hand, the heat transfer between the two fluids inside any preheater can be expressed by [26, 27]:

$$\frac{d}{dt}Q_i = A_{in,i}.\left\{U_{in,i}.\frac{d}{dt}\Delta Tm_i + \Delta Tm_i\,.\frac{d}{dt}U_{in,i}\right\} \tag{21}$$

where the temperature difference between the two fluids along the heat transfer surface area is not fixed, so the log mean temperature difference (ΔT_m) can be used to evaluate the heat transfer rate, as follows, [28]:

$$\Delta Tm_i = \frac{T_{f,i+1} - T_{f,i-1}}{\ln\left(\frac{T_{v,\mathrm{i}} - T_{f,i-1}}{T_{v,\mathrm{i}} - T_{f,i+1}}\right)} \tag{22}$$

The heat transfer rate in the condenser is calculated by the same technique used above in the preheater.

3.6 Mathematical Model of the Heat Transfer Coefficients

The time derivative of the overall heat transfer coefficient can be calculated by [26, 27]:

$$\frac{d}{dt}\left(\frac{1}{U_{in,i}}\right) = \frac{d}{dt}\left(\frac{1}{h_{in,i}}\right) + \frac{d_{in}.\ln\left(d_o/d_{in}\right)}{2}.\frac{d}{dt}\left(\frac{1}{k_{m,i}}\right) + \frac{d_{in}}{d_o}.\frac{d}{dt}\left(\frac{1}{h_{o,i}}\right) \tag{23}$$

3.6.1 Heat transfer coefficients in the condenser and preheaters

The dynamic equation of the outer heat transfer coefficients in the preheaters and condenser given by:

$$\frac{d}{dt}h_{o,i} = 0.729\left(\frac{g}{d_{o,i}N_{VD,i}}\right)^{1/4}.\frac{d}{dt}\left(\frac{\rho_{l,i}(\rho_{l,i}-\rho_{v,i})h^*_{fgo,i}k^3_{l,i}}{\mu_{l,i}(T_{V,i}-T_{W,i})}\right)^{1/4}$$

$$= 0.182\left(\frac{g}{N_{VD,i}d_{o,i}}\right)^{1/4}.\frac{(T_{V,i}-T_{W,i})^{-2}}{\mu^2_{l,i}}\left(\frac{\rho_{l,i}(\rho_{l,i}-\rho_{v,i})h^*_{fgo,i}k^3_{l,i}}{\mu_{l,i}(T_{V,i}-T_{W,i})}\right)^{-3/4}\left(\begin{array}{l}\mu_{l,i}(T_{V,i}-T_{W,i})\left(\begin{array}{l}3\rho_{l,i}(\rho_{l,i}-\rho_{v,i})h^*_{fgo,i}k_{l,i}{}^2\frac{d}{dt}k_{l,i}\\+k^3_{l,i}\left(\begin{array}{l}\rho_{l,i}(\rho_{l,i}-\rho_{v,i})\frac{d}{dt}h^*_{fgo,i}\\+h^*_{fgo,i}\left(\begin{array}{l}\rho_{l,i}\left(\frac{d}{dt}\rho_{l,i}-\frac{d}{dt}\rho_{v,i}\right)\\+(\rho_{l,i}-\rho_{v,i})\frac{d}{dt}\rho_{l,i}\end{array}\right)\end{array}\right)\end{array}\right)\\-\rho_{l,i}(\rho_{l,i}-\rho_{v,i})h^*_{fgo,i}k^3_{l,i}\left(\begin{array}{l}\mu_{l,i}\left(\frac{d}{dt}T_{V,i}-\frac{d}{dt}T_{W,i}\right)\\+(T_{V,i}-T_{W,i})\frac{d}{dt}\mu_{l,i}\end{array}\right)\end{array}\right) \quad (24)$$

where ρ, k, μ, N_{VD} are respectively the density, conductivity, dynamic viscosity, and the number of tubes rows in the vertical direction, while the subscripts l, v, w refer respectively to liquid, vapor, and tube wall.

The time derivative of the modified latent heat of vaporization is:

$$\frac{d}{dt}h^*_{fgo,i} = \frac{d}{dt}h_{fgo,i} + 0.68\left\{cp_{l,i}.\left(\frac{d}{dt}T_{v,i}-\frac{d}{dt}T_{w,i}\right)+\left(T_{v,i}-T_{w,i}\right).\frac{d}{dt}cp_{l,i}\right\} \quad (25)$$

On the other hand, the time derivative heat transfer coefficient of fluid inside the tubes can be calculated by, [29]:

$$\frac{d}{dt}h_{in,i} = \frac{1}{d_{in,i}}\left(Nu_{in,i}.\frac{d}{dt}k_{in,i}+k_{in,i}.\frac{d}{dt}Nu_{in,i}\right) \quad (26)$$

3.6.2 Heat transfer coefficients in the effects

The dynamic equation of the heat transfer coefficients inside the evaporator's tubes given by:

$$\frac{d}{dt}h_{in,i} = 0.139\left(\frac{g}{N_{VD,i}.d_{in,i}}\right)^{1/4}\frac{(T_{v,i}-T_{w,i})^{-2}}{\mu^2_{l,i}}\left[\frac{\rho_{l,i}\left(\rho_{l,i}-\rho_{v,i}\right)k^3_{l,i}}{\mu_{l,i}\left(T_{v,i}-T_{w,i}\right)}h^*_{fgin,i}\right]^{-3/4}\left(\begin{array}{l}\mu_{l,i}(T_{v,i}-T_{w,i})\left(\begin{array}{l}3\rho_{l,i}(\rho_{l,i}-\rho_{v,i})h^*_{fgin,i}k_{l,i}{}^2.\frac{d}{dt}k_{l,i}\\+k^3_{l,i}\left(\begin{array}{l}\rho_{l,i}(\rho_{l,i}-\rho_{v,i})\frac{d}{dt}h^*_{fgin,i}\\+h^*_{fgin,i}\left(\begin{array}{l}\rho_{l,i}\left(\frac{d}{dt}\rho_{l,i}-\frac{d}{dt}\rho_{v,i}\right)\\+(\rho_{l,i}-\rho_{v,i})\frac{d}{dt}\rho_{l,i}\end{array}\right)\end{array}\right)\end{array}\right)\\-\rho_{l,i}(\rho_{l,i}-\rho_{v,i})h^*_{fgin,i}k^3_{l,i}\left(\begin{array}{l}\mu_{l,i}\left(\frac{d}{dt}T_{v,i}-\frac{d}{dt}T_{w,i}\right)\\+(T_{v,i}-T_{w,i})\frac{d}{dt}\mu_{l,i}\end{array}\right)\end{array}\right) \quad (27)$$

And the time derivative of the modified latent heat is:

$$\frac{d}{dt}h^*_{fgin,i} = \frac{d}{dt}h_{fgin,i} + 0.375\left\{cp_{l,i}.\left(\frac{d}{dt}T_{v,i} - \frac{d}{dt}T_{w,i}\right) + \left(T_{v,i} - T_{w,i}\right).\frac{d}{dt}cp_{l,i}\right\} \quad (28)$$

Finally, through the tube, the time derivative of mass flow rate evaluated using the mean velocity by:

$$\frac{dM_i}{dt} = A_{in,i}(\rho_{in,i}.\frac{d}{dt}V_{in,i} + V_{in,i}\frac{d}{dt}\rho_{in,i}) \quad (29)$$

4. Model Validation

The developed model using Engineering Equation Solver (EES) software is validated by comparing the results with data reported from two models, the first one developed by El-Dessouky and Ettouney [1], and the second developed by Abdelkareem [30]. Table 2 shows the important input parameters for simulation, output parameters obtained from each model, and the error between the output parameters of the proposed model in this paper and the output parameters of the above-mentioned models. The validity of the proposed model shows perfect agreement with data in the literature, with maximum error does not exceed 5.0%, so the proposed model is valid to accurately predict the performance parameters of FF-MED-TVC plant.

Table 2
Validation of FF-MED-TVC proposed model with data reported from two model in the literature

Parameter 2	El-Dessouky [1]	FF-MED-TVC	Error %	Abdelkareem [30]	FF-MED-TVC	Error %
Number of effects	4		-	4		-
Inlet feed salinity, (ppm)	42000		-	42000		-
Outlet brine salinity, (ppm)	70000		-	70000		-
Top brine temperature, (°C)	56.67		-	56.67		-
last brine temperature, (°C)	40		-	40		-
Feed temperature, (°C)	35		-	35		-
The feed water temperature leaving the last preheater,	51.54		-	51.54		-
Seawater temperature, (°C)	25		-	25		-
Motive steam pressure (k.Pa)	250		-	250		-
Compressed vapor temperature, (°C)	60		-	60		-
Motive steam flow rate kg/s	0.19			0.19		
Distillate production, (kg/s)	1	0.9806	1.94	0.967	0.9806	1.40
Gain output ratio (GOR)	5.263	5.161	1.93	5.09	5.161	1.36
Brine flow kg/s	1.5	1.519	1.26	1.453	1.519	4.54
Feed flow kg/s	2.5	2.5	0	2.42	2.5	3.3
Steam flow rate to the first effect	0.275	0.2764	0.51	0.2804	0.2764	1.42
Entrained vapor kg/s	0.085	0.0863	1.53	0.0904	0.0863	4.53
Entrainment Ratio for TVC	2.228	2.199	1.30	2.1	2.199	4.71

5. Results and Analysis

Steady-state and dynamic model was developed for the proposed plant, to investigate the model's response under various operating conditions. In particular, the effects of variation of (i) motive steam pressure, (ii) seawater flow rate and (iii) seawater temperature were investigated. A

general overview of the steady-state model predicting is given in Fig. (4), where the distribution along the effects of some of the main operating parameters was shown.

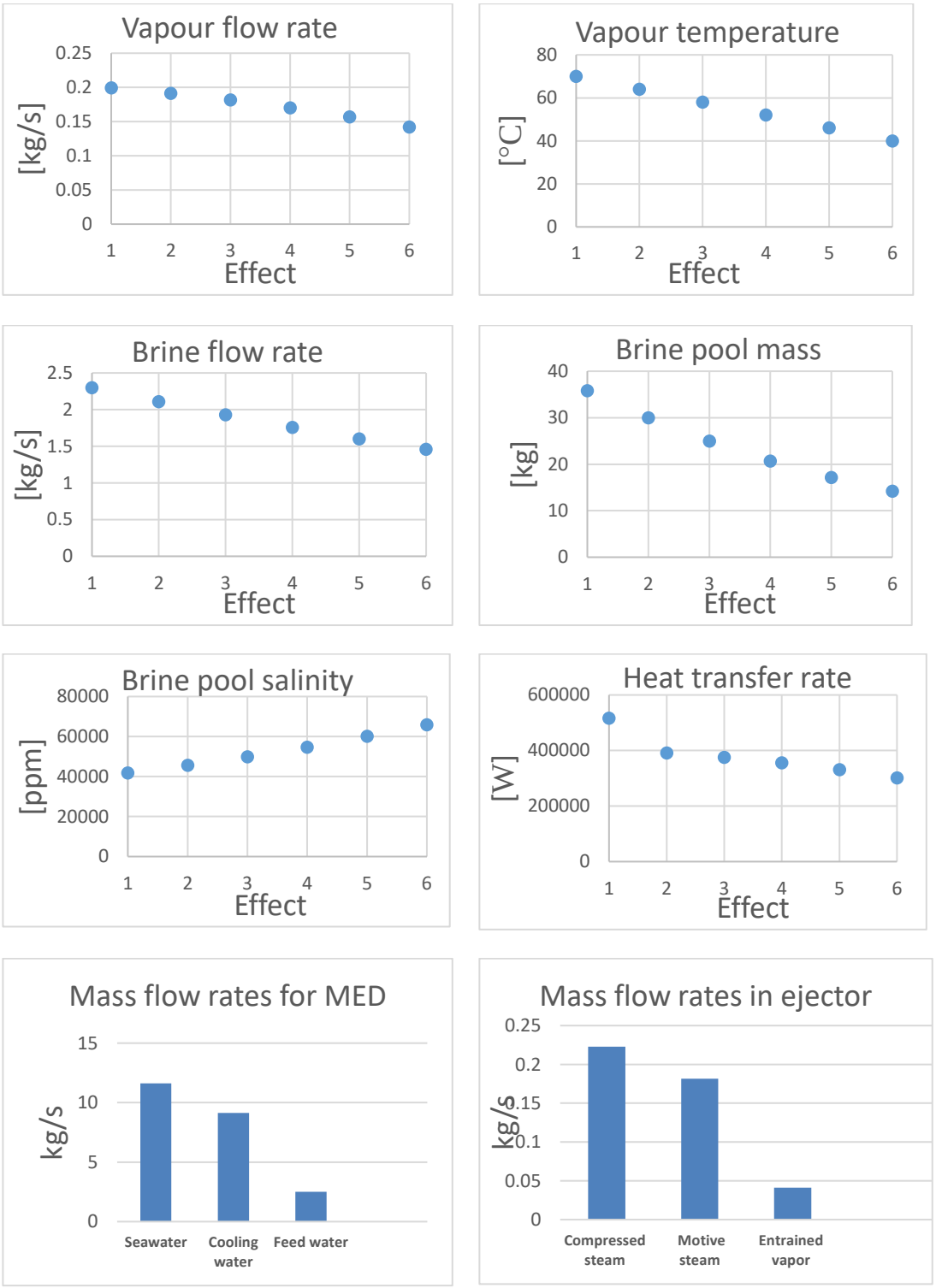

Fig. 4. Predicted trends of main operating variables along the effects in case of steady state

5.1 Effect of a Variation in the Motive Steam Pressure

Variation in the motive steam pressure is one of the most important controlling parameter in MED-TVC plants, where this parameter clearly affects the total efficiency, productivity, performance ratio (PR), and gain output ratio (GOR) of the plant. The sudden change of this parameter is highly probable especially when the motive steam is coming from the solar heat exchanger.

This section discusses the dynamic behavior due to an increase of 0.2 bar (10 % disturbance) rectangular pulse forcing function on 2 bar of the motive steam pressure, which continued only for 10 seconds after the 20 seconds of steady operation, as shown in Figure 5.

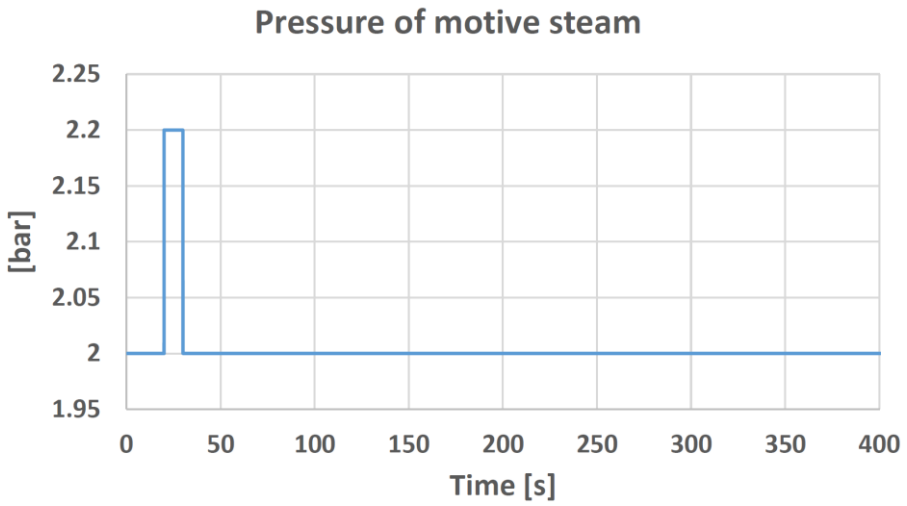

Fig. 5. Disturbance employed of the pulse forcing function of the motive steam pressure

Figure 6 is the prediction of the system's response to a change in the motive steam pressure. The increase in the motive steam pressure leads to an increase in the mass flow rate of motive steam through the ejector (from 0.182kg/s up to 0.198 kg/s), but the mass flow rate of entrained vapor from the last effect decreases (from 0.041 kg/s to 0.036kg/s), (fig 6a). This is because when the pressure of the motive steam at the inlet of the nozzle rises, and for Mach number in nozzle's throat equal to one, the pressure in the nozzle's throat will increase, thus the pressure at the outlet of the nozzle will increase. As a result, the pressure difference between the outlet of the nozzle and the entrained vapor from the last effect will decrease, so that the mass flow rate of entrained vapor from this effect will be reduced, and entrainment ratio will decrease (from 0.228 to 0.184), (fig 6i).

The mixed steam in the ejector comes out with a higher mass flow rate, as well as pressure and temperature, (fig 6, a, b), thus the amount of heat provided to the first effect will rise, which will raise the temperature and the amount of generated steam in this effect (from 0.2 kg/s up to 0.207 kg/s). Consequently, the productivity of generated steam in the rest effects will rise, (fig 6, c, d), except for the last effect, where the mass flow rate of entrained steam from this effect will decrease (as mentioned previously). Therefore, the pressure and temperature will rise in the last effect, which leads to a reduction in the heat transfer driving force and thus the mass flow rate of generated steam will decrease (from 0.142 kg/s to 0.139 kg/s).

The reduction of the entrained steam from the last effect leads to slight increase in the mass flow rate of steam that will reach the condenser and thus the temperature of the seawater leaving the condenser will increase slightly, where the heat transfer rate in the condenser will increase from (243.2 kw up to 246.3 kw), (fig 6,e,f). Additionally, the higher productivity of generated steam, except

for the last effect, means a very small decrease in the height of the water within each effect, which is equivalent to a very small decrease in the mass flow rate of brine with a very small increase in salinity, (fig 6 g, h). There is almost no effect on the performance of the preheater, as the temperature of the seawater leaving the condenser will increase slightly before entering the last preheater, so that the feed water can enter to the first effect with a slight rise, (Figure 6(j)).

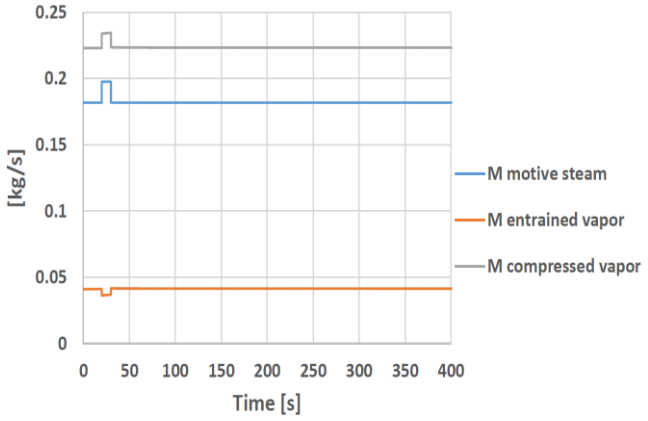

(a)

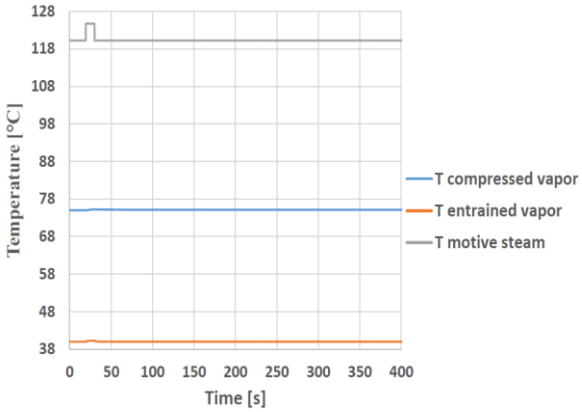

(b)

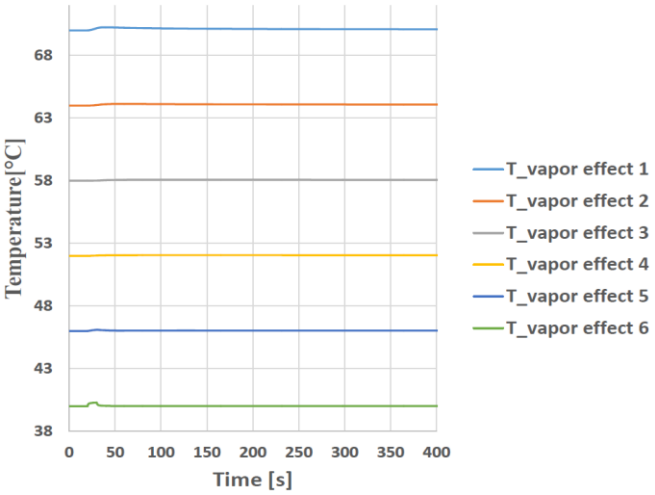

(c)

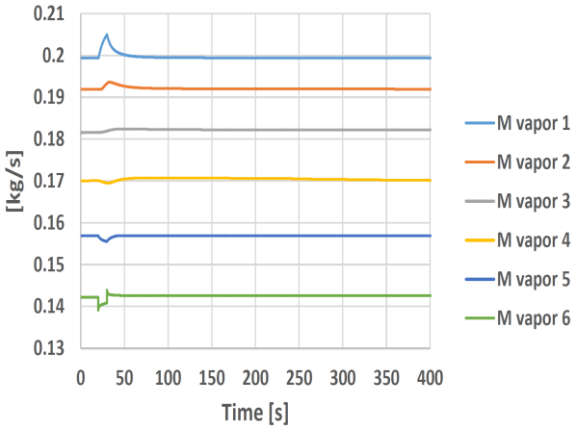

(d)

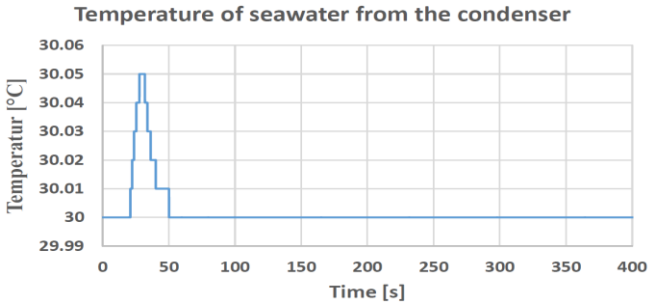

(e)

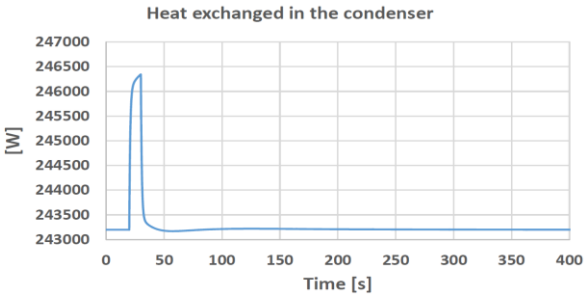

(f)

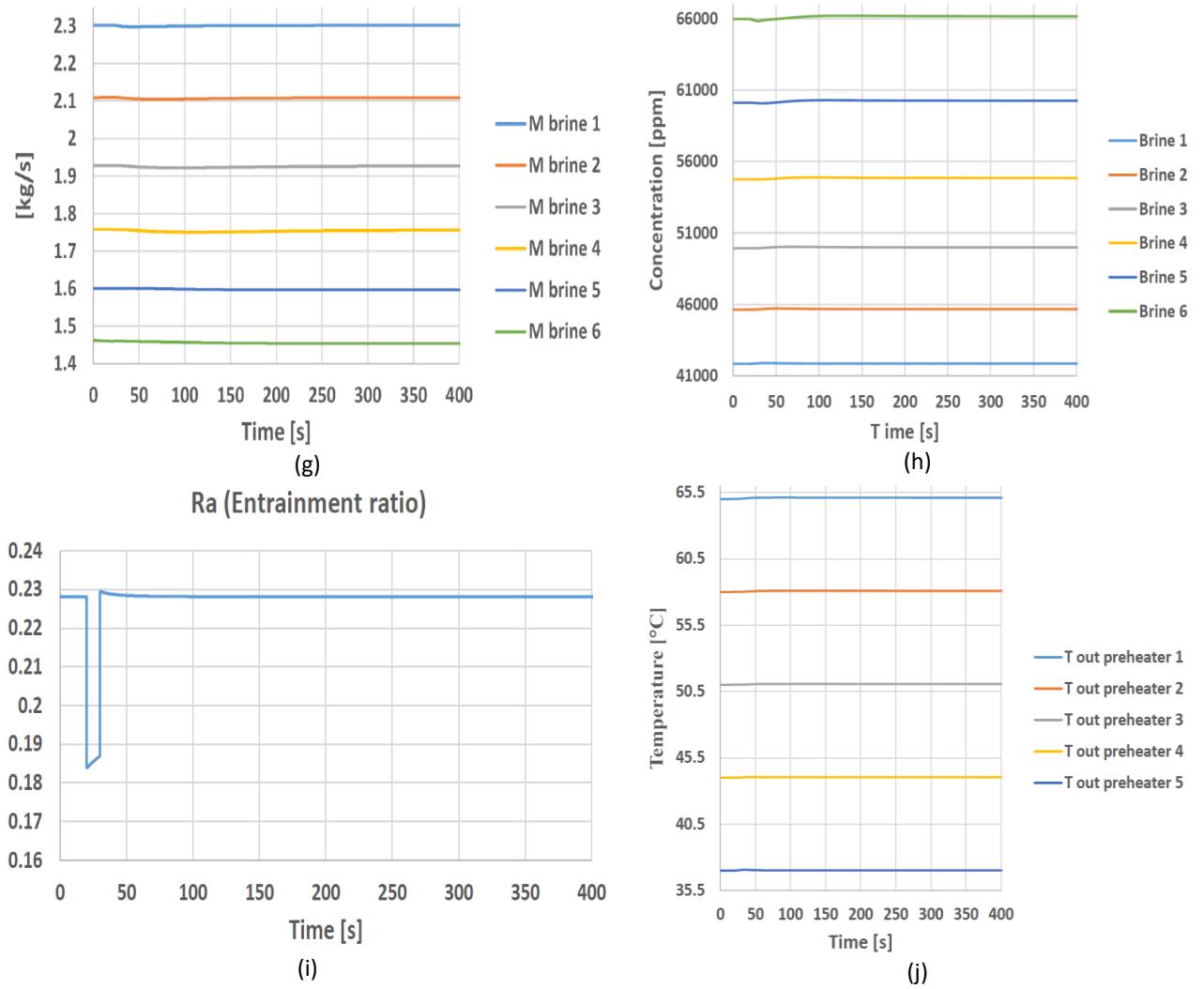

Fig. 6. Transient response of the system to a rectangular pulse forcing function on the motive steam pressure (+10 % disturbance)

5.2. Effect of a Variation in the Seawater Mass Flow Rate

This section discusses the dynamic behavior prompted by an increase of 1.162 kg/s (10 % disturbance) rectangular pulse forcing function on 11.62 kg/s of the seawater mass flow rate, which continued only for 10 seconds after the 20 seconds of steady operation, as shown in Figure 7.

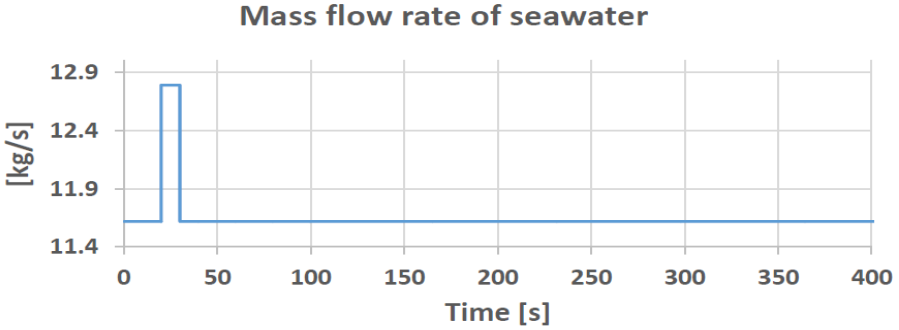

Fig. 7. Disturbance employed of the pulse forcing function of seawater mass flow rate

Figure 8 is the prediction of the system's response to a change in seawater mass flow rate entering the condenser. The increase in the mass flow rate of seawater leads to a decrease in the temperature of the water leaving the condenser, (Figure 8(a)), despite of the increase in the heat exchange rate in the condenser in the beginning (from 243.2 kw up to 245.5 kw) as a result of the increase in the log mean temperature difference between steam and water inside the condenser tubes (Figure 8(b)). It is worth noting that after the effect of disturbance reaches the last effect, the amount of generated steam that will be produced from the last effect will decrease (Figure 8(c)), thus the amount of vapor reaching the condenser will decrease, and thus the heat exchange rate in the condenser will decrease to 242.2 kw until it returns to the stability value.

On the other hand, this disturbance leads to a decrease in the pressure and temperature of the generated steam in each effect, (Figure 8(d)). Additionally, the productivity of generated steam in each effect will decrease, (Figure 8(c)), as a result of two reasons. The first one is that the pressure drop in the last effect will lead to a decrease in the amount of entrained vapor from this effect by the ejector (from 0.0411kg/s to 0.0398 kg/s); consequently, the decrease in the heat supplied to first effect (Figure 8(e)). The second reason is that the decrease in the saturation temperatures which result a higher amount of latent heat needed to evaporate the same amount of steam.

The temperature of feed water leaving each preheater will decrease, (Figure 8(f)), as a result of the sudden huge increase of feed water entering each preheater (from 2.5 kg/s up to 3.67 kg/s), in the same time, lower productivity and saturation temperature in each effect of generated steam which will be used to heat up the feed water in each preheater. Consequently, the feed water temperature to the first effect decreases. This disturbance leads to an increase in the brine level in each effect, because the feed water mass flow rate to the first effect will increase and the productivity of each effect will decrease, and as a result the mass flow rate of brine in each effect will increase, (Figure 8(g)). It can be noted that the curve representing the mass flow rate of brine from the first effect takes a sharp jump similar to the disturbance curve because the first effect is directly under this disturbance.

Finally, the concentration of brine will decrease in each effect, where the concentration of salts decreases more and more in the successive effects as a result of the decrease in the generated steam within each effect (Figure 8(h)).

5.3 Effect of a Variation of the Seawater Inlet Temperature

This section discusses the dynamic behavior prompted by 2.5°C increase (10 % disturbance) rectangular pulse forcing function on 25°C of the seawater temperature, which continued only for 10 seconds after the 20 seconds of steady operation as shown in Figure 9.

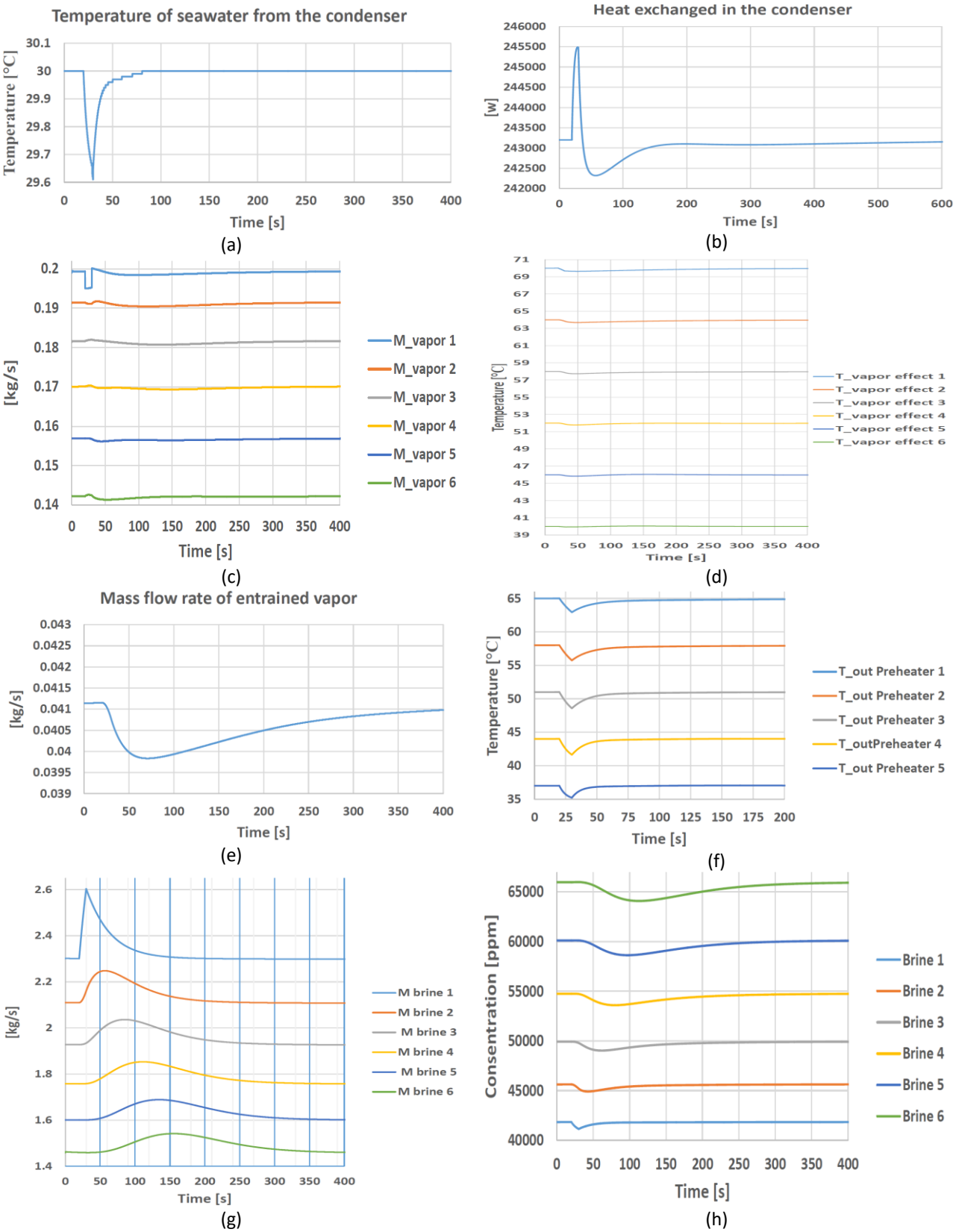

Fig. 8. Transient response of the system to a rectangular pulse forcing function on the seawater mass flow rare (+10 % disturbance)

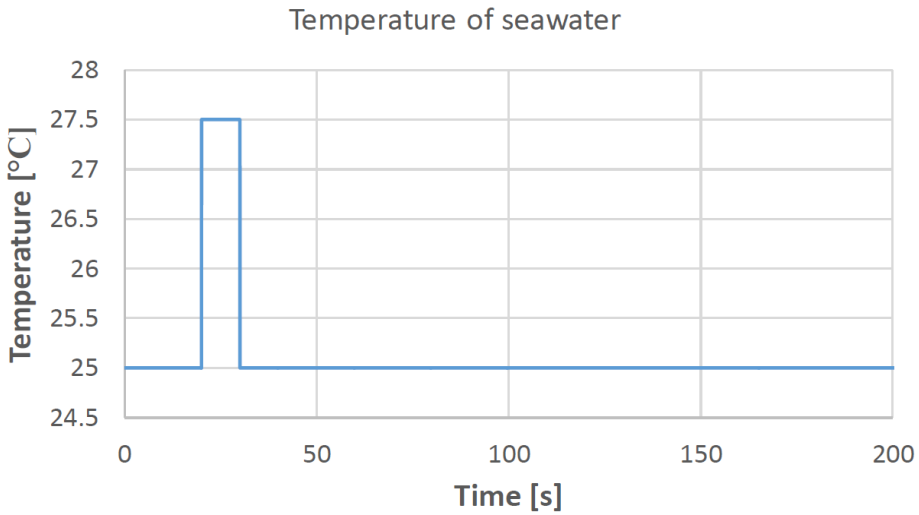

Fig. 9. Disturbance employed of the pulse forcing function of seawater temperature

Figure 10 is the prediction of the system's response to a change in seawater temperature entering the condenser. The increase in the temperature of seawater leads to an increase in the temperature of the seawater leaving the condenser (from 30°C up to 31.61°C), (Figure 10(a)), despite of the decrease in the heat exchange rate in the condenser (from 234.2 kw to 216.7 kw) as a result of the decrease in the log mean temperature difference between steam and water inside the condenser tubes, (Figure 10(b)).

As mentioned above, the temperature of the seawater leaving the condenser will increase as a result of an increase in its entry temperature, this will lead to increase in the temperature of the feed water entering each preheater, and thus the amount of heat exchanged in each preheater will decrease as a result of the decrease in the log mean temperature difference in each preheater, (Figure 10(g)).

The feed water temperature of the first effect increase, this leads to an increase in the pressure and temperature of the brine pool and generated steam in the first effect, and the same goes for the rest of the effects (Figure 10(d)). However, it is noted that the rise in the pressure and temperature in the last effect is relatively higher than the rest of the effects and this response in the last effect occurs before the rest of the effects, as a result of the decrease of vapor condensation rate in the condenser (from 0.101 kg/s to 0.09 kg/s), (Figure 10(h)), resulting from the decrease in the log mean temperature difference, as mentioned above. Therefore, part of the steam coming from the last effect to the condenser will not condense, which raises the pressure and temperature in the condenser and thus the pressure and temperature rise in the last effect, which is connected directly to the condenser. As a result, the heat transfer driving force in each effect will decrease, (i.e., heat exchange rate decreases in each effect), and consequently the yield of each effect of generated steam will decrease, (Figure 10(e)).

The small decrease in the mass flow rate of generated steam in each effect leads to a very small increase in the brine level in each effect; consequently, the mass flow rate of brine in each effect will increase slightly, (Figure 10(c)). Finally, the concentration of salts will decrease as a result of the decrease in generated steam in each effect, and it is noted that the decrease in the concentration of salts in the last effect is relatively higher than the rest of the effects because the decrease in generated steam in this effect is relatively higher than the rest of the effects, (Figure 10(f)).

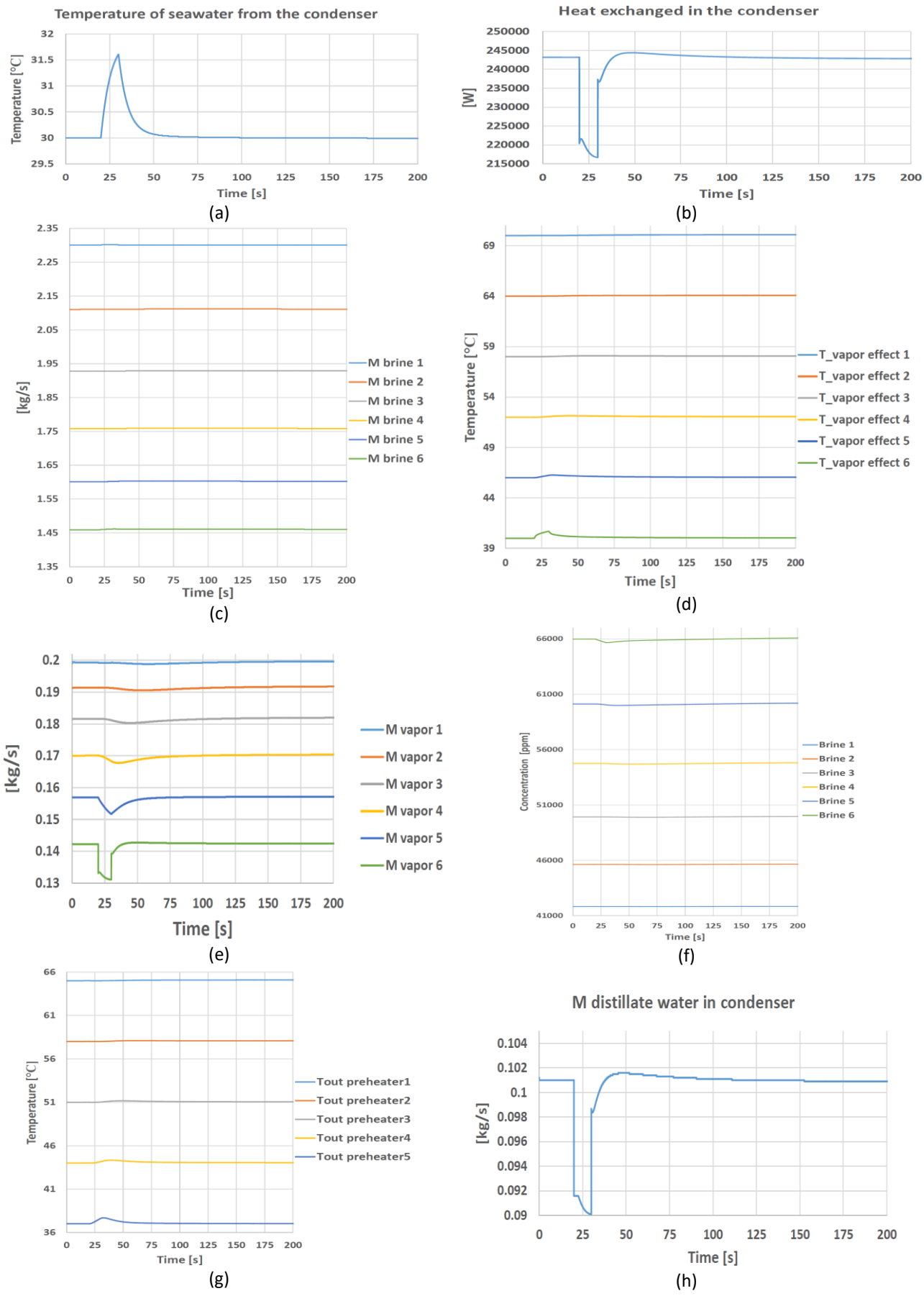

Fig. 10. Transient response of the system to a rectangular pulse forcing function on the seawater temperature (+10 % disturbance)

6. Conclusion

In this paper a dynamic mathematical model for the FF-MED-TVC desalination plant has been developed. Engineering Equation Solver (EES) software was employed to solve the proposed model which is based on the basic balance equations of mass, salt and energy flows. The model is validated against the steady-state performance by comparing the results with data reported from two models in the literature. The maximum error between the outputs was not more than 5%, therefore the proposed model can be used to predict the transient behavior of the desalination plant. After validation, the model has been utilized to predict the dynamic response on 10% disturbance caused by rectangular pulse forcing function on some of the most important parameters to get the optimal design of system and a clearer view in control applications.

For the same percentage (10%) for the three studied disturbances, the station takes the longest time to return to 95 % of steady state in the case of increasing of seawater mass flow rate, (about 350 seconds after the turbulence is removed), while it takes the shortest time to return to 95 % of steady state in the case of increasing the pressure of motive steam (about 50 seconds after the turbulence is removed).

References

[1] El-Dessouky, Hisham T., and Hisham Mohamed Ettouney. *Fundamentals of salt water desalination*. Elsevier, 2002.

[2] Askari, Ighball Baniasad, and Mehran Ameri. "The application of linear Fresnel and parabolic trough solar fields as thermal source to produce electricity and fresh water." *Desalination* 415 (2017): 90-103. https://doi.org/10.1016/j.desal.2017.04.005

[3] Baniasad Askari, I., and M. Ameri. "Solar Rankin cycle (SRC) powered by linear Fresnel solar field and integrated with combined MED desalination system." *Renew. Energy* 117 (2018): 52-70. https://doi.org/10.1016/j.renene.2017.10.033

[4] Alelyani, Sami M., Nicholas W. Fette, Ellen B. Stechel, Pinchas Doron, and Patrick E. Phelan. "Techno-economic analysis of combined ammonia-water absorption refrigeration and desalination." *Energy Conversion and Management* 143 (2017): 493-504. https://doi.org/10.1016/j.enconman.2017.03.085

[5] Amin, Zakaria Mohd, and M. N. A. Hawlader. "Analysis of solar desalination system using heat pump." *Renewable Energy* 74 (2015): 116-123. https://doi.org/10.1016/j.renene.2014.07.028

[6] Esfahani, Iman Janghorban, and Changkyoo Yoo. "A highly efficient combined multi-effect evaporation-absorption heat pump and vapor-compression refrigeration part 2: Thermoeconomic and flexibility analysis." *Energy* 75 (2014): 327-337. https://doi.org/10.1016/j.energy.2014.07.082

[7] Baniasad Askari, I., and M. Ameri. "Techno economic feasibility analysis of MED/TVC desalination unit powered by linear fresnel solar field direct steam." *Desalination* 394 (2016): 1-17. https://doi.org/10.1016/j.desal.2016.04.022

[8] ElHelw, Mohamed, Wael M. El-Maghlany, and Walaa M. El-Ashmawy. "Novel sea water desalination unit utilizing solar energy heating system." *Alexandria Engineering Journal* 59, no. 2 (2020): 915-924. https://doi.org/10.1016/j.aej.2020.03.019

[9] Cipollina, A., M. Agnello, A. Piacentino, A. Tamburini, B. Ortega, P. Palenzuela, D. Alarcon, and G. Micale. "A dynamic model for MED-TVC transient operation." *Desalination* 413 (2017): 234-257. https://doi.org/10.1016/j.desal.2017.03.005

[10] Elsayed, Mohamed L., Osama Mesalhy, Ramy H. Mohammed, and Louis C. Chow. "Transient performance of MED processes with different feed configurations." *Desalination* 438 (2018): 37-53. https://doi.org/10.1016/j.desal.2018.03.016

[11] Guo, Yali, Minle Bao, Luyuan Gong, and Shengqiang Shen. "Effects of preheater arrangement on performance of MED desalination system." *Desalination* 496 (2020): 114702. https://doi.org/10.1016/j.desal.2020.114702

[12] El-Dessouky, Hisham T., Hisham M. Ettouney, and Faisal Mandani. "Performance of parallel feed multiple effect evaporation system for seawater desalination." *Applied Thermal Engineering* 20, no. 17 (2000): 1679-1706. https://doi.org/10.1016/S1359-4311(99)00098-8

[13] Shen, Shengqiang, Shihe Zhou, Yong Yang, Luopeng Yang, and Xiaohua Liu. "Study of steam parameters on the performance of a TVC-MED desalination plant." *Desalination and water treatment* 33, no. 1-3 (2011): 300-308. https://doi.org/10.5004/dwt.2011.2653

[14] Alamolhoda, F., R. KouhiKamali, and M. Asgari. "Parametric simulation of MED–TVC units in operation." *Desalination and Water Treatment* 57, no. 22 (2016): 10232-10245. https://doi.org/10.1080/19443994.2015.1038735
[15] Hanafi, A. S., G. M. Mostafa, A. Fathy, and A. Waheed. "Thermo-economic analysis of combined cycle MED-TVC desalination system." *Energy Procedia* 75 (2015): 1005-1020. https://doi.org/10.1016/j.egypro.2015.07.342
[16] Askari, I. Baniasad, and Mohamad Ameri. "Thermodynamic analysis of multi effect desalination unit with thermal vapor compression feed by different motive steam pressures." *Desalination and Water treatment* 184 (2020): 57-71. https://doi.org/10.5004/dwt.2020.25387
[17] Elsayed, Mohamed L., Osama Mesalhy, Ramy H. Mohammed, and Louis C. Chow. "Exergy and thermo-economic analysis for MED-TVC desalination systems." *Desalination* 447 (2018): 29-42. https://doi.org/10.1016/j.desal.2018.06.008
[18] Aly, Narmine H., and M. A. Marwan. "Dynamic response of multi-effect evaporators." *Desalination* 114, no. 2 (1997): 189-196. https://doi.org/10.1016/S0011-9164(98)00011-3
[19] Mazini, Mohammad Taghi, Alireza Yazdizadeh, and Mohammad Hossein Ramezani. "Dynamic modeling of multi-effect desalination with thermal vapor compressor plant." *Desalination* 353 (2014): 98-108. https://doi.org/10.1016/j.desal.2014.09.014
[20] Guimard, L., A. Cipollina, B. Ortega-Delgado, G. Micale, F. Couenne, P. Bandelier, and C. Jallut. "New considerations for modelling a MED-TVC plant under dynamic conditions." *Desalination* 452 (2019): 94-113. https://doi.org/10.1016/j.desal.2018.10.026
[21] Dong, Zhe, Miao Liu, Xiaojin Huang, Yajun Zhang, Zuoyi Zhang, and Yujie Dong. "Dynamical modeling and simulation analysis of a nuclear desalination plant based on the MED-TVC process." *Desalination* 456 (2019): 121-135. https://doi.org/10.1016/j.desal.2019.01.020
[22] Georgiou, Marios C., and Aristides M. Bonanos. "A transient model for forward and parallel feed MED." *Desalination and Water Treatment* 57, no. 48-49 (2016): 23119-23131. https://doi.org/10.1080/19443994.2016.1180480
[23] Elsayed, Mohamed L., Osama Mesalhy, Ramy H. Mohammed, and Louis C. Chow. "Effect of disturbances on MED-TVC plant characteristics: Dynamic modeling and simulation." *Desalination* 443 (2018): 99-109. https://doi.org/10.1016/j.desal.2018.05.021
[24] Khan, Ambareen, Nurul Musfirah Mazlan, Mohd Azmi Ismail, and Mohammad Nishat Akhtar. "Experimental and numerical simulations at sonic and supersonic Mach numbers for area ratio 7.84." *CFD Letters* 11, no. 5 (2019): 50-60.
[25] Khan, Sher Afghan, Abdul Aabid, Fharukh Ahmed Mehaboobali Ghasi, Abdulrahman Abdullah Al-Robaian, and Ali Sulaiman Alsagri. "Analysis of area ratio in a CD nozzle with suddenly expanded duct using CFD method." *CFD Letters* 11, no. 5 (2019): 61-71.
[26] Hassan, Ashraf S., and Abdalla S. Hanafi. "Dynamic Behavior of Multiple Effect Distillation with the Disturbance of Seawater Mass Flow Rate." In *IDA World Congress, Maspalomas, Gran Canaria, Spain*, pp. 21-26. 2007.
[27] A. A. Tahawy, Dynamic Modeling and Performance Analysis of Solar MED Desalination by Dynamic Modeling and Performance Analysis of Solar MED Desalination System, Ph.D Thesis, Faculty of Engineering, Cairo University, 2014.
[28] Omar, Hossin, Suliman Alfarawi, Azeldin El-sawi, and Hassan Alobeidy. "Study the Effect of Baffle Spacing on Heat Transfer and Pressure Drop in Shell and Tube Heat Exchanger." *Journal of Advanced Research in Numerical Heat Transfer* 6, no. 1 (2021): 22-30.
[29] Fekadu, Birlie, and H. V. Harish. "Numerical Studies on Thermo-Hydraulic Characteristics of Turbulent Flow in a Tube with a Regularly Spaced Dimple on Twisted Tape." *CFD Letters* 13, no. 8 (2021): 20-31. https://doi.org/10.37934/cfdl.13.8.2031
[30] M. E. Abdelkareem, Dynamic behavior and performance of different types of multi-effect desalination plants, Ph.D Thesis, Faculty of Engineering, Central Florida University, 2019.